INNOVATION FOREVER
Open Access

Innovation Discovery
ISSN 2959-5150 (Online)

Short Communication

Enhanced the Electrochemical Stability of Al-Zn-Mg Alloy Through the Dual Incorporation of ZrO_2 and V_2O_5 into the Alumina Layer

Mosab Kaseem[1*], Arash Fattah-alhosseini[2*]

[1]*Corrosion and Electrochemistry Laboratory, Department of Nanotechnology and Advanced Materials Engineering, Sejong University, Seoul, South Korea*
[2]*Department of Materials Engineering, Faculty of Engineering, Bu-Ali Sina University, Hamedan, Iran*

[*]***Correspondence to: Mosab Kaseem, PhD, Assistant Professor,*** *Corrosion and Electrochemistry Laboratory, Department of Nanotechnology and Advanced Materials Engineering, Sejong University, 98 Gunja-dong, Gwangjin-gu, Seoul, 05006, South Korea. Email: mosabkaseem@sejong.ac.kr*
Arash Fattah-alhosseini, PhD, Professor, *Department of Materials Engineering, Faculty of Engineering, Bu-Ali Sina University, Hamedan 65178-38695, Iran. Email: a.fattah@basu.ac.ir*

Abstract

This study explores the impact of direct and indirect incorporation of metallic oxide particles namely ZrO_2 and V_2O_5 on the corrosion behavior of the alumina layer obtained by the plasma electrolytic oxidation of Al-Zn-Mg alloy. To achieve this goal, plasma electrolytic oxidation coating was formed in an alkaline-aluminate-ZrO_2 electrolyte, without and with NH_4VO_3. The morphological analysis reveals a porous structure influenced by gas bubble discharge and rapid cooling, featuring micro-pores, oxide nodules, and cracks. The incorporation of V_2O_5 particles is observed to decrease surface roughness and enhance the compactness of the oxide layer. The X-ray diffraction patterns reveal the presence of γ-Al_2O_3, α-Al_2O_3, ZrO_2, and V_2O_5 particles exclusively in the sample coated in the electrolyte with NH_4VO_3. Potentiodynamic polarization and impedancetests in a 3.5 wt.% NaCl solution revealed enhanced corrosion resistance, attributed to reduced micro-defects through V_2O_5 and ZrO_2 incorporation.

Keywords: Al alloy, plasma electrolytic oxidation, V_2O_5, ZrO_2, corrosion

Received: December 24, 2023
Revised: February 1, 2024
Accepted: February 20, 2024
Published: March 15, 2024

Citation: Kaseem M, Fattah-alhosseini A. Enhanced the Electrochemical Stability of Al-Zn-Mg Alloy Through the Dual Incorporation of ZrO_2 and V_2O_5 into the Alumina Layer. *Innov Discov*, 2024; 1(1): 2.

1 INTRODUCTION

Aluminum and its alloys are well-recognized for their excellent structural properties in various industries, including aircraft, architecture, transportation, and manufacturing, thanks to features such as low density and high mechanical strength. Despite these advantages, the limited surface hardness and corrosion resistance of Al alloys have restricted their extensive application[1]. The advent of plasma electrolytic oxidation (PEO) has become a notable surface engineering technology, generating significant interest. PEO oxide coatings exhibit remarkable corrosion protection properties[2-7]. The properties of oxide films produced through PEO are significantly impacted by factors such as the chemical composition of the electrolyte and electrical parameters, including current density, frequency, and current mode[8-12]. Recent research has underscored the potential for substantial improvement in corrosion resistance, particularly in demanding environments where micro-arc-induced pores are only partially filled. This enhancement is achieved through the incorporation of stable metal oxides like V_2O_5, SiO_2, CeO_2, TiO_2, and ZrO_2 as secondary particles into the oxide layer. For instance, Arunnellaiappan et al.[13] demonstrated a noteworthy enhancement in the corrosion resistance of Al-Zn-Mg alloy through the

introduction of CeO_2, as evidenced by potentiodynamic polarization experiments. Bahramian et al.[14] found that the inclusion of TiO_2 particles in the oxide coating, formed in an alkaline-silicate solution, elevated the corrosion resistance of an Al-Zn-Mg alloy. In a separate study, Xiang et al.[15] observed that the addition of potassium fluorozirconate salts to an alkaline electrolyte facilitated the integration of ZrO_2 into oxide layers, thereby improving the corrosion characteristics of the 6063 Al alloy. Fatimah et al.[16] successfully incorporated SiO_2 and ZrO_2 particles into the PEO coating formed on 6061Al alloy. They reported that electrophoresis is the primary mechanism influencing the incorporation of these particles into the coating layer.

Additionally, V_2O_5 particles were incorporated into the electrolyte during the PEO processing of Al alloys to induce dark hues and enhance the electrochemical stability of the resulting coatings[17-19]. For example, Kwon et al.[17] demonstrated enhanced electrochemical stability and reduced porosity in 6061 Al alloy by incorporating V_2O_5 particles into the coating. These particles, known for their electrochemical inertness, created a more effective barrier against corrosive chlorine ions, thereby inhibiting corrosion. Similarly, Kaseem et al.[19] improved the compactness and electrochemical stability of Al alloy by introducing V_2O_5 nanoparticles into the coating, utilizing an alkaline-phosphate electrolyte. While past studies primarily focused on the incorporation of single particles, our study aims to integrate both V_2O_5 and ZrO_2 particles into the Al_2O_3 oxide film formed on Al-Zn-Mg alloy through PEO. This will be achieved using an electrolyte containing NH_4VO_3 metallic salt and ZrO_2 powder. To the best of our knowledge, this is the first instance of incorporating ZrO_2 and V_2O_5 particles into the alumina layer produced via PEO treatment of Al-Zn-Mg alloy. In this study, we successfully fabricated Al_2O_3-ZrO_2-V_2O_5 oxide layers on Al-Zn-Mg alloy using the PEO process with an alkaline-aluminate electrolyte containing ZrO_2 and NH_4VO_3. The characteristics of the resulting oxide layers were analyzed in terms of structure, composition, and corrosion behavior.

2 MATERIALS AND METHODS

The material under investigation in this study is an Al-Zn-Mg alloy (7075 alloy) with the following chemical composition: 5.1% Zn, 2.2% Mg, 1.2% Cu, 0.3% Fe, 0.2% Si, 0.2% Cr, 0.2% Mn, with the remaining balance being Al in weight percent. Before the PEO treatment, the specimens underwent grinding and polishing using abrasive paper, followed by degreasing with pure acetone. Two electrolytes, designated as Bath A (6g/L KOH + 4g/L $NaAlO_2$ + 2gr of ZrO_2 nanoparticles) and Bath B (6g/L KOH + 4g/L $NaAlO_2$ + 2g/L ZrO_2 + 3gr NH_4VO_3), were employed in the PEO process. The concentration of ZrO_2 nanoparticles was adjusted to 3g to prevent particle agglomeration, a phenomenon that may occur at higher concentrations. The PEO procedures were conducted for 180 seconds at a frequency of 60Hz and a current density of 100mA/cm^2 under alternating current conditions. Throughout the PEO process, the temperature of the electrolytes was maintained at 288 K. Surface and cross-sectional morphologies of the oxide layer were analyzed using a Scanning Electron Microscope (SEM-HITACHI, S-4800) equipped with an energy-dispersive spectrometer (EDS). Additionally, atomic force microscopy (AFM-3D surface profiler, Contour GT-K 3D) was employed in ambient air to measure mean surface roughness (Ra) using a 10 nm radius silicon tip in contact mode. The thickness of the oxide layer was measured using an eddy-current tester (Minitest 2100, Electrophysik, Germany), with a minimum of 10 measurements conducted on each side of the sample. X-ray diffraction (XRD) was conducted using a RIGAKU D-MAX 2500 instrument with a step size of 0.05° and a scan range of 30 to 90° to identify the component phases. The chemical compositions of the PEO-coated oxides were analyzed using X-ray photoelectron spectroscopy (XPS, VG Microtech, ESCA2000). The corrosion resistance of the oxide films was assessed through potentiodynamic polarization tests and electrochemical impedance spectroscopy (EIS) in a 3.5% NaCl solution, with the sample serving as the working electrode, an Ag/AgCl electrode as the reference electrode, and a platinum plate as the counter electrode. The potentiodynamic polarization tests were conducted within a range from -0.25 to -0.4V vs. open circuit potential (OCP) at a scan rate of 1mV/s, with the samples immersed in the corrosive solution for 1h to achieve OCP stabilization. EIS measurements were conducted over a frequency range from 10^6Hz to 0.1Hz, with data sampled at intervals of 10 points per decade, using a 10mV rms amplitude. To ensure data accuracy, these tests were repeated three to four times.

3 RESULTS AND DISCUSSION

3.1 Morphology of the Coating

The surface properties of the oxide coating formed on the Al-Zn-Mg alloy after 180 seconds in Baths A and B are depicted in Figure 1. Both oxide films exhibit distinctive porous architectures characterized by micro-pores and oxide nodules resulting from gas bubble discharge through discharge channels during intense arcing. Surface cracks appear in both samples because of the rapid cooling of oxide clusters upon contact with the electrolyte held at 288K[20]. As shown in Figure 1A and 1B, the sample from Bath A exhibits more noticeable cracks compared to the sample from Bath B. In contrast, it is evident from Figure 1D and 1E that the oxide layer produced in Bath B exhibits lower porosity and smaller pore size compared to its counterparts in Bath A. The varied surface morphologies of the oxide coatings in Baths A

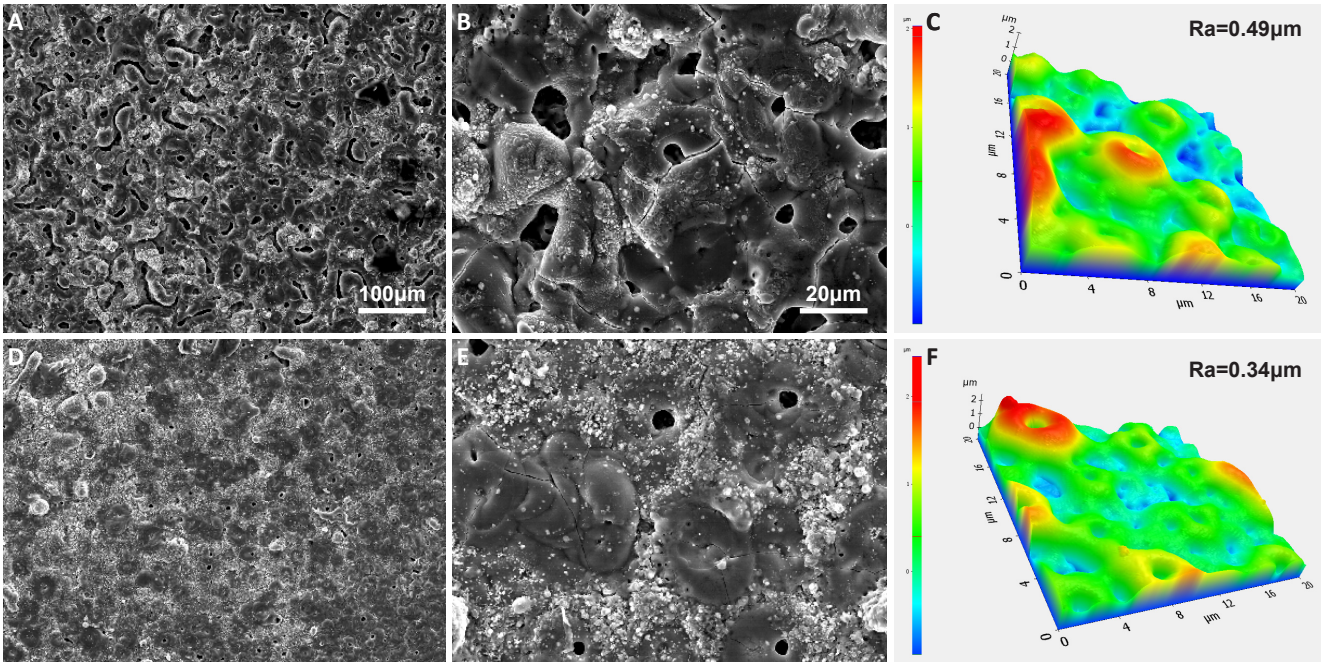

Figure 1. SEM images showing surface morphologies (lower and higher magnification) and the corresponding AFM results of the oxide layers formed on Al-Zn-Mg alloy via PEO in (A-C) Bath A and (D-F) Bath B.

and B would be ascribed to differences in electrolyte content and other electrochemical reactions during the PEO process, leading to the incorporation of V-based compounds in the majority of micropores and cracks. The AFM results in Figure 1C and 1F show that the surface roughness values of the PEO coatings obtained in Baths A and B were ~0.49μm and ~0.34μm, respectively. This suggests that the oxide layer's surface roughness in Bath B was somewhat lower than that in Bath A. The observed variation in surface roughness between the coatings obtained in Baths A and B is attributed to the incorporation of V_2O_5 nanoparticles, as will be elucidated later. The formation of micropores during the PEO process, attributed to the implosion of gas bubbles, plays a crucial role in determining surface roughness and is closely associated with electrical transport behavior[21,22]. Upon incorporating V_2O_5 into the oxide layer, there is a notable decrease in the electric resistivity compared to the case of the oxide layer in Bath A[23]. This reduction in resistivity signifies improved electrical conductivity, leading to the effective consumption of high energy generated from plasma discharges in the development of a surface with lower roughness. The intricate interplay between gas bubble dynamics, electrical properties, and surface morphology underscores the influence of V_2O_5 incorporation on the characteristics of the oxide coatings obtained in Bath B. Examination of the EDS data provided in Table 1 highlights discernible differences in the compositions of oxide films obtained from Baths A and B. Although the oxide film obtained from Bath B contains elements such as Al, O, and Zr, it has a distinct composition compared to that observed in Bath A. In addition, the presence of V elements in Bath B can also be attributed to the incorporation of V compounds because of the addition of NH_4VO_3 additive in the electrolyte. On the other hand, the average thickness was calculated to be 7.54±0.1μm and 7.33±0.2μm, for the samples made in Bath A and Bath B, respectively. This suggests that the impact of V_2O_5 on the thickness of oxide layers was negligible. This observation can be attributed to the consistent application of a constant current density of 100mA/cm^2 across both samples for a duration of 180s[24].

Figure 2 presents the cross-sectional images of the oxide films formed in Baths A and B. Both coatings were composed of an outer porous layer and an inner layer (as marked by arrows), and the thickness of the coating layers was approximately identical (~7.4±0.3mμ) which was nearly identical to the results calculated by the eddy-current tester. In addition, the sample coated in Bath A exhibited a rough surface with relatively coarse pores and some cracks, as shown in Figure 2A. In contrast, Figure 2B indicated that the sample coated in Bath B had a relatively uniform compact microstructure with fewer micropores, which was consistent with the surface images in Figure 1.

3.2 Composition of the Coating and the Mechanism of Incorporation

Figure 3 depicts the XRD patterns of oxide films formed on an Al-Zn-Mg alloy in Baths A and B. The oxide film produced in Bath A predominantly comprises γ-Al_2O_3 (JCPDS card no: 01-077-2135), α-Al_2O_3 (JCPDS card no: 01-075-0783), Al (JCPDS card no: 00-001-1180) phases, and ZrO_2 (JCPDS card no: 01-079-1768).

Table 1. Composition of the oxide layers formed on Al-Zn-Mg alloy via PEO in Baths A and B detected through EDS

Sample	Al (wt.%)	O (wt.%)	Zr (wt.%)	V (wt.%)
Bath A	43.36±3.42	48.15±4.67	8.49±7.75	-
Bath B	38.21±2.75	49.37±4.89	5.97± 0.61	6.45± 0.63

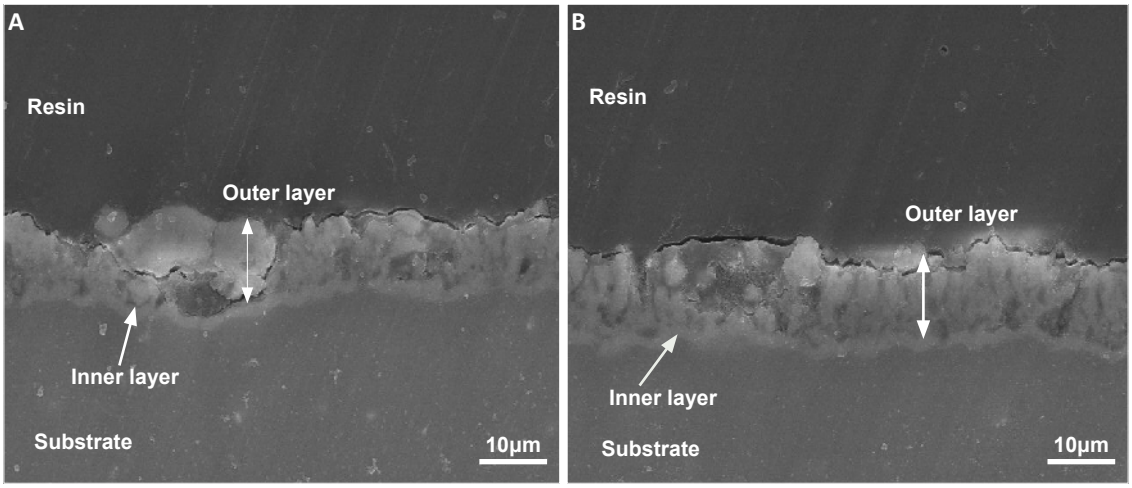

Figure 2. SEM images showing the cross-sectional images the oxide layers formed on Al-Zn-Mg alloy via PEO in (A) Bath A and (B) Bath B.

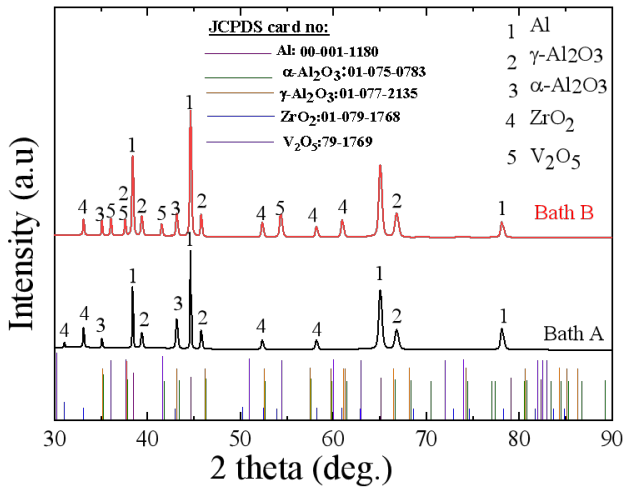

Figure 3. XRD results of the oxide layers formed on Al-Zn-Mg alloy via PEO in Baths A and B.

According to Equation 1 and Equation 2, α-Al_2O_3 and γ-Al_2O_3 are formed through the counter migration of Al^{3+} and O^{-2} within the oxide layer, depending on the cooling rates.

The presence of tetragonal-structured ZrO_2 in the XRD patterns indicates the successful incorporation of ZrO_2 into the oxide films during the PEO process. Through the electrochemical anodic reaction (Equation 4), V_2O_5 (JCPDS card no: 79-1769) is formed[25]. The electrochemical processes during PEO can be succinctly described as follows:

$$2Al^{3+} + 3O^{2-} \xrightarrow{\text{Rapid-cooling}} \gamma - Al_2O_3 \ (1)$$

$$2Al^{3+} + 3O^{2-} \xrightarrow{\text{Slow-cooling}} \alpha - Al_2O_3 \ (2)$$

$$NH_4VO_3 \rightarrow NH_4^{+} + VO_3^{-} \ (3)$$

$$2Al^{3+} + 6VO_3^{-} \rightarrow Al_2O_3 + 3V_2O_5 \ (4)$$

To investigate the chemical nature, composition, and oxidation states of Al, O, Zr, and V in the samples, XPS measurements were utilized. The full-range XPS spectral analysis of the oxide films produced in Baths A and B is presented in Figure 4A. Both samples exhibit the presence of Al, O, and Zr, with the additional detection of V in the coating obtained from Bath B. Notably, there are no significant differences in the fundamental elements observed between both samples, except for the inclusion of V in the sample obtained from Bath B. The Al, O, and Zr elements are attributed to the oxidation of the Al alloy substrate in an alkaline-aluminate electrolyte solution containing ZrO_2 nanoparticles.

The individual spectra of O1s and Zr3d in the coating from Bath A, and O1s, Zr3d, and V2p in the coating from Bath B, are displayed in Figure 4B-F. In Figure 4B, the O1s spectrum of the oxide film from Bath A fits well with Al_2O_3 and ZrO_2, corresponding to binding energies of 530.9 and 531.9eV, respectively. Deconvolution of Zr3d (Figure 4C) reveals two peaks at approximately 184.8 and 182.4eV, indicative of Zr–O bonding in ZrO_2[26]. In contrast, the O1s spectrum of the Bath B coating (Figure 4D) exhibits three peaks at 530.9, 531.9, and 529.6eV, attributed to Al_2O_3, ZrO_2, and V_2O_5, respectively. Similarly, the Zr3d spectrum of the Bath B coating (Figure 4E) shows two peaks at around 184.8 and 182.4eV, indicating ZrO_2 incorporation. The

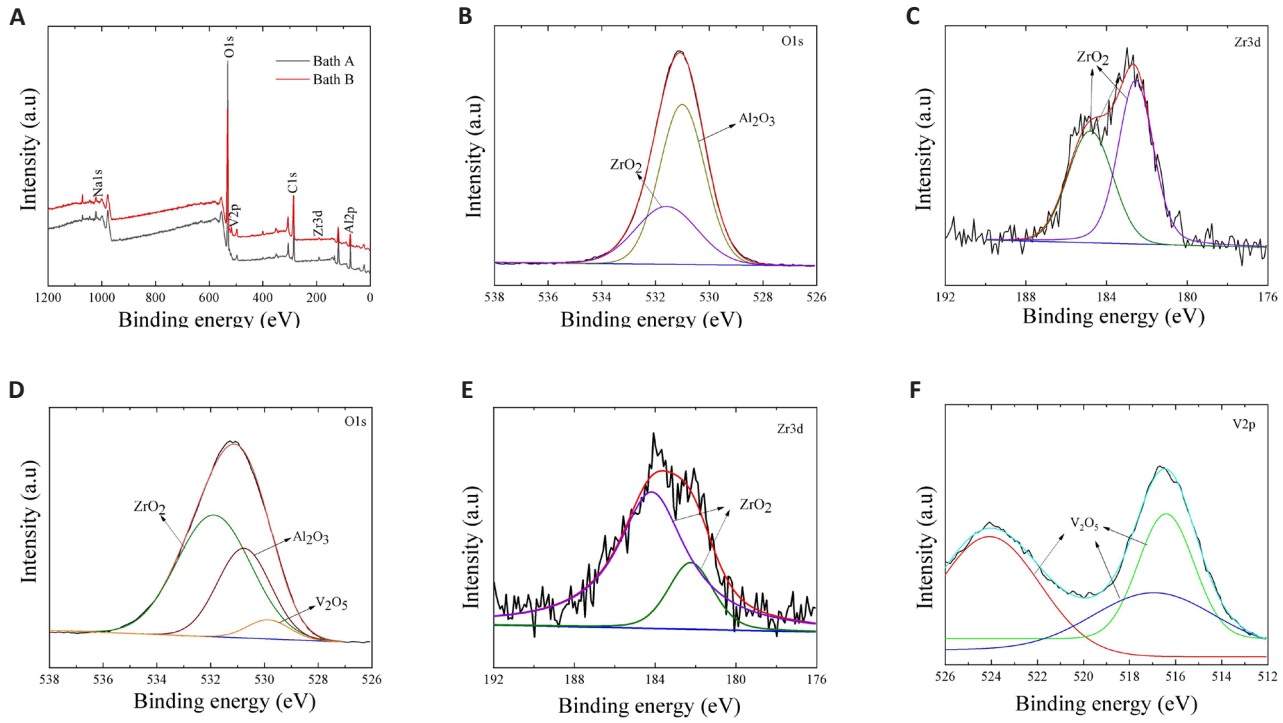

Figure 4. XPS results of the oxide layers formed on Al-Zn-Mg alloy via PEO in Baths A and B. A: XPS full scan of the oxide layers made from Baths A and B. B and C: High-resolution XPS spectra of O1s (B) and Zr3d (C) spectra on the surface of the sample obtained from Bath A. D-F: O1s (D), Zr3d (E), and V2p (F) spectra on the surface of the sample coated in Bath B.

presence of V_2O_5 in the Bath B coating is confirmed by the V2p peak (Figure 4F), which splits into two peaks at approximately 517 and 525eV, corresponding to V 2p 3/2 and V 2p 1/2, respectively. Fitting analysis reveals three peaks at 517, 517.4, and 524.3eV, characteristic of V_2O_5[27,28].

Figure 5 illustrates a proposed mechanism for the incorporation of ZrO_2 and V_2O_5 particles, based on the structural morphologies and composition of the oxide layers. ZrO_2 particles dispersed in the electrolyte would exhibit a negative zeta potential[28]. This negative surface charge facilitated the electrophoretic migration of the ZrO_2 particles toward the anode surface during the PEO process. The incorporation of ZrO_2 particles into the oxide layer occurred due to localized melting induced by the high-temperature conditions generated during plasma arcing. Consequently, the assimilation of ZrO_2 can be primarily attributed to the combined effects of electrophoresis and physical mixing (Figure 5A). In Bath B, the incorporation of ZrO_2 followed the same mechanism described in Bath A. In addition, the inclusion of NH_4VO_3 powders in the electrolyte results in the efficient incorporation of V_2O_5 particles, a fact suggested in the XRD diagrams by the separate peaks corresponding to V_2O_5 compounds. In this case, the incorporation of V_2O_5 particles occurs through a series of plasma-assisted electrochemical reactions (Figure 5B). VO_3^- ions are generated by ionizing NH_4VO_3 metallic salt in the electrolyte (Equation 3), and, propelled by the strong electric field created during PEO, these ions migrate towards the anode surface, where they react with Al^{3+} ions to form V_2O_5 particles according to Equation 4.

3.3 Corrosion Behavior of the Coatings

Potentiodynamic polarization curves in a 3.5 wt.% NaCl solution were presented in Figure 6A to assess the corrosion resistance of the substrate and the oxide layers formed in Baths A and B. The corrosion potential (E_{corr}) and corrosion current density (i_{corr}) were calculated using the Tafel extrapolation method, while polarization resistance values (R_p) were determined using the Stern-Geary equation (Equation 5).

$$R_p = \frac{\beta_a . \beta_c}{2.303 i_{corr} (\beta_a + \beta_c)} \quad (5)$$

In this equation, β_a and β_c represent the anodic and cathodic Tafel slopes, respectively[29]. Table 2 summarizes the results obtained from these investigations. Irrespective of the coating type, both samples treated in Baths A and B demonstrated superior corrosion resistance compared to the untreated substrate. The bare substrate exhibited the most negative E_{corr}, the largest i_{corr}, and the lowest R_p, indicating significantly poorer corrosion resistance in comparison to the coated samples. However, compared with samples exposed in Bath A, the E_{corr} of the oxide layer developed in Bath B showed a substantial shift to a more positive zone (-0.642 V vs. Ag/AgCl). Furthermore, the i_{corr} for the oxide layers in Bath B was two orders of magnitude lower than that in Bath A,

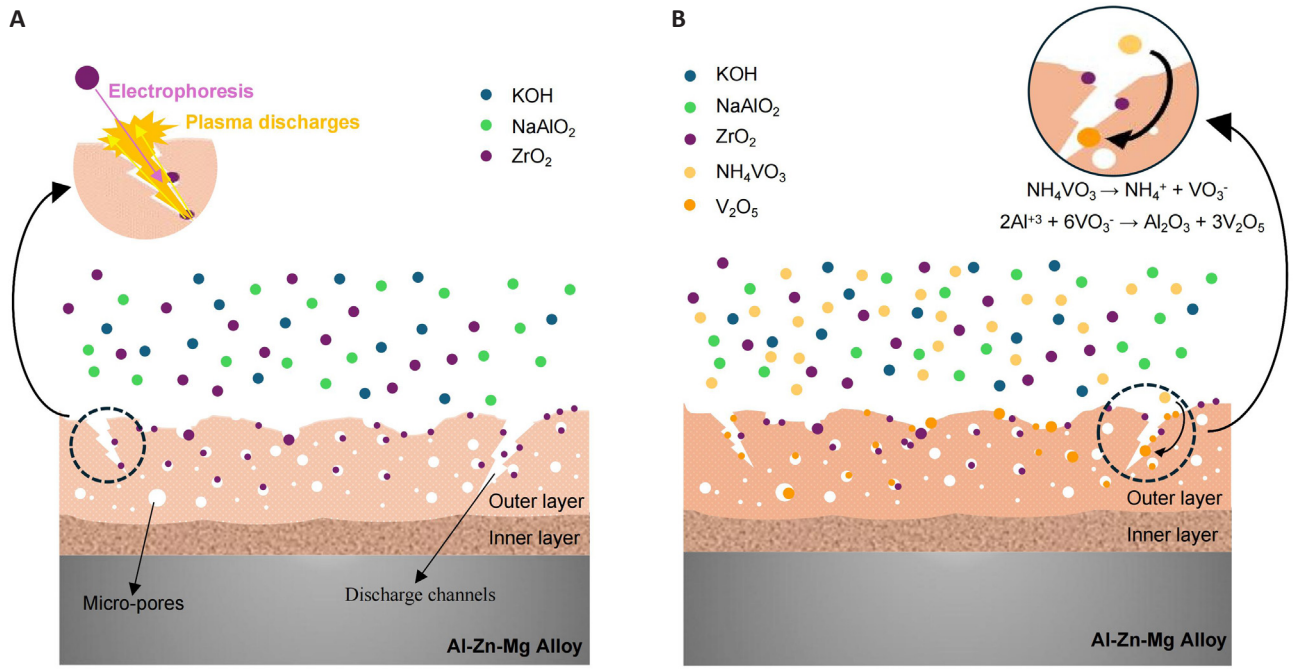

Figure 5. Schematic illustration for the incorporation mechanism of ZrO_2 and V_2O_5 particles into Al_2O_3 layer where (A) Bath A and (B) Bath B.

indicating that the sample coated in Bath B had a much-reduced corrosion rate. This difference shows that the sample in Bath B has improved corrosion resistance, reflected by a higher value of *Rp*, which may be related to the alteration of the surface structure of the oxide coating caused by the incorporation of V_2O_5.

For comparison, the i_{corr} values of different oxide films formed on Al alloys via PEO were collectively plotted, considering the types of secondary particles incorporated into the oxide layer, as depicted in Table 3[13-16,30,31]. In Table 3, it is evident that, regardless of variations in electrolyte and electrical parameters, the oxide layer formed in Bath B, following the current strategy, consistently demonstrated the lowest i_{corr} values compared to other investigated cases. This was observed even under shorter coating times and conditions of medium current density during the coating formation. This leads to the conclusion that the incorporation of ZrO_2 and V_2O_5 particles into the oxide layer represents an effective method for enhancing the corrosion resistance of Al alloy via PEO.

EIS assessments were also performed in a 3.5 wt.% NaCl solution after a 1h immersion, aiming to elucidate the role of V_2O_5 within the coating obtained from Bath B. The impedance spectra, featured in both Nyquist and Bode configurations, are presented in Figure 6B and 6C for detailed examination. In Figure 6B (Nyquist plot), a semi-circular feature was evident, notably more pronounced in the oxide layer derived from Bath B compared to those from Bath A. Additionally, the Nyquist plots displayed linear behavior with a 45° inclination at low-frequency regions, indicating potential ion diffusion and corrosion product migration within the coating-substrate interface during the corrosion test[32,33]. Moreover, the impedance modulus |Z| at the low frequency region (0.1 Hz) serves as an indicator of the overall resistance of the oxide layers[34]. In Figure 6C, the oxide layer produced in Bath B demonstrated a higher |Z| compared to its Bath A counterpart, suggesting enhanced corrosion resistance in the former. This enhancement is primarily attributed to the incorporation of V_2O_5, which effectively fills structural defects within the PEO coating, consequently obstructing micro-pores and amplifying the impedance response of the oxide layer.

The EIS data was interpreted through the utilization of equivalent circuits as illustrated in Figure 6D, with the respective values of circuit elements outlined in Table 4. Within the proposed circuit models, R_s, R_o, and R_i delineate the resistances of the corrosive solution, outer, and inner layers, while CPE_o and CPE_i signify the constant phase elements corresponding to the outer and inner layers, respectively. Additionally, a Warburg element (*W*) was incorporated in series with R_i to simulate the mass-transport diffusion of Cl^- ions through the oxide layers.

As evident from Table 4, the values of R_o and R_i for the oxide layer produced in Bath B surpassed those of Bath A. This suggests that the corrosion resistance of the oxide layers improved with the integration of V_2O_5 into the coating. Additionally, irrespective of the electrolyte concentration, R_i exceeded R_o, likely owing to the denser structure of the inner layer, with Bath B exhibiting higher R_i values compared to those from

Table 2. Results of Potentiodynamic Polarization Tests of the Bare Substrate and the Oxide Layers Immersed in a 3.5 wt.% NaCl Solution for 1h

Sample	E_{corr} (V)	i_{corr} (A/cm^2)	β_a (V/decade)	β_c (V/decade)	R_p (Ωcm^2)
Substrate	-0.780	5.92×10^{-7}	0.155	-0.151	5.61×10^{4}
Bath A	-0.694	3.10×10^{-9}	0.153	-0.160	1.10×10^{7}
Bath B	-0.642	2.95×10^{-11}	0.169	-0.149	1.17×10^{9}

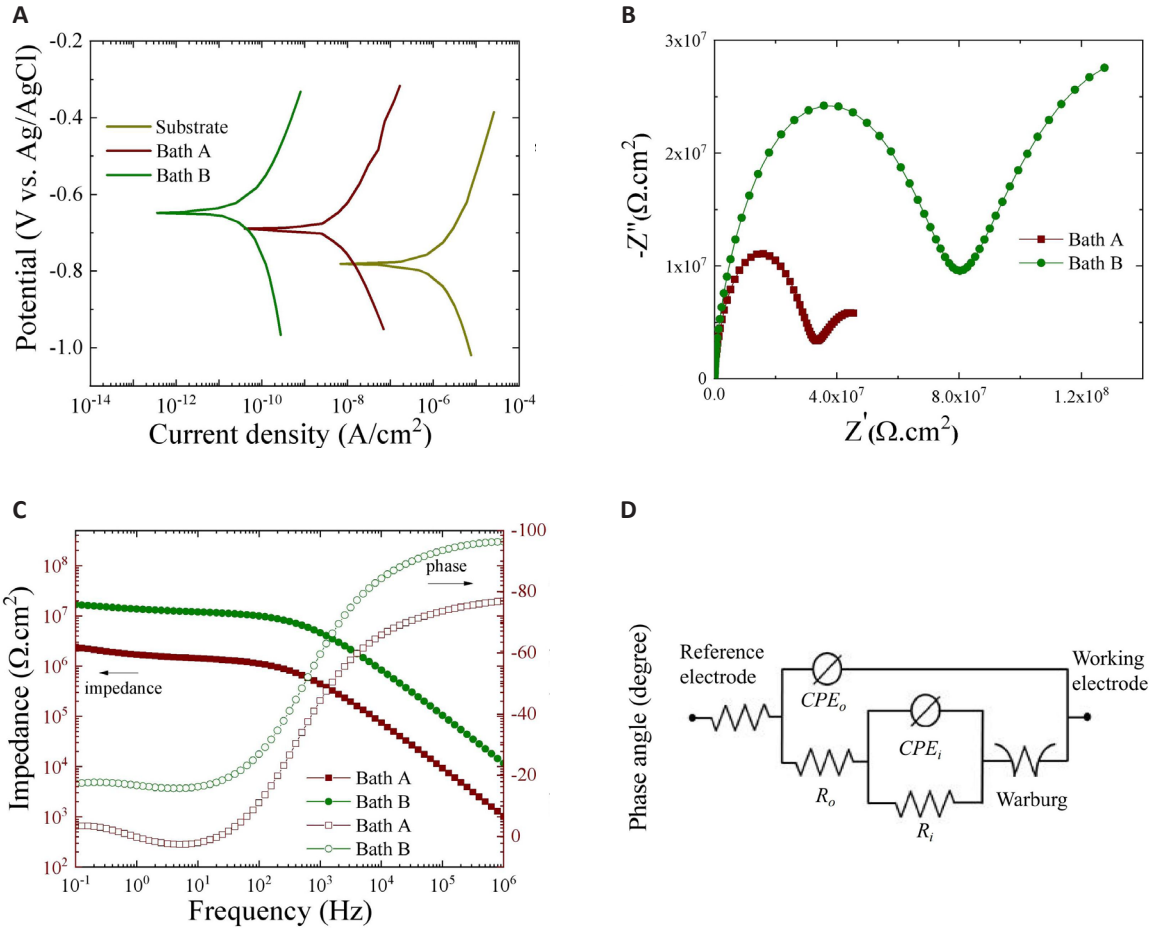

Figure 6. Corrosion results of the substrate, and the oxide layers formed via PEO in Baths A and B. A-C: (A) Potentiodynamic polarization curves of the bare substrate and the oxide layers formed on Al-Zn-Mg alloy via PEO in Baths A and B (B and C) Nyquist and Bode plots of the oxide layers formed on Al-Zn-Mg alloy via PEO in Baths A and B where (B) Nyquist plots and (C) Bode plots. D: The equivalent circuit model used for fitting EIS results.

Bath A. This behavior is likely due to the advantageous effects of ZrO_2 and V_2O_5 incorporation, which contribute to blocking micro-pores. Additionally, these particles exhibit strong chemical stability in neutral electrolytes like 3.5 wt.% NaCl solution, impeding the transport of corrosive ions toward the substrate during corrosion testing. Previous studies have shown that either ZrO_2[35,36] or V_2O_5[17,18] nanoparticles can act as corrosion inhibitors by replacing water molecules at the surface/coating interface. The reduced porosity and smaller size of micro-pores observed in the oxide layer formed in Bath B compared to Bath A can be attributed to the incorporation of V_2O_5, leading to improved corrosion resistance. On the other hand, Table 4 revealed also higher values of n_0 and n_i in Bath B compared to Bath A, suggesting a smoother coating/substrate interface facilitated by V_2O_5 integration which was in good agreement with the roughness results shown in Figure 1. Meanwhile, *CPE-Y_0* represents the dielectric behavior at the electrolyte/coating interface[34], with the Bath A sample exhibiting a higher *CPE-Y_0* value than its Bath B counterpart.

4 CONCLUSION

The incorporation of ZrO_2 and V_2O_5 into the oxide layer of an Al-Zn-Mg alloy through PEO has yielded significant insights into the composition and corrosion resistance of the resulting coatings. Both oxide films contained elements Al, O, and Zr, while the V element was detected only in the oxide film obtained from Bath B due to the presence of the NH_4VO_3 additive. The introduction of V_2O_5, facilitated by NH_4VO_3 metallic salt ionization, and ZrO_2, integrated through electrophoresis and physical mixing, has played a pivotal role in

Table 3. Studies Reported by Previous Researchers about the Influence of Inorganic and Organic Additives on the Surface Properties of PEO Coatings Formed on Al Alloys

Substrate	Type of additive	additive content (g/L)	PEO conditions	I_{corr} (A/cm^2)	Highlights	Ref.
AA7075	CeO_2	4	Current density: 150mA/cm^2 Electrolyte: alkaline-silicate electrolyte Coating time: 10min	1.25×10^{-10}	Incorporation of CeO_2 nanoparticles increased also the adhesion strength of the coating–substrate system	[13]
AA7075	TiO_2	4	Current density: 150mA/cm^2 Alkaline-silicate electrolyte Coating time: 60min	1.5×10^{-7}	Microhardness increased with rising nanoparticle concentration.	[14]
6063 Al alloy	ZrO_2	2	Current density: 5,10, 15, 20A/cm^2 Alkaline-silicate electrolyte Coating time: 18min	6.688×10^{-8}	The PEO coating at 15A/dm^2 had superior microstructure and thickness, with fewer defects	[15]
6061 Al alloy	SiO_2/ZrO_2	2.5 of each SiO_2 and ZrO_2	Current density: 130mA/cm^2 Alkaline-phosphate electrolyte Coating time: 10min	8.21×10^{-10}	Porosity decreased by about 2.62% with either SiO_2 or ZrO_2 nanoparticles and by 7.61% with both.	[16]
7075 Al alloy	CNT	150 mL/L	Current density: 150mA/cm^2 Alkaline-silicate-fluoride electrolyte Coating time: 10min	8.33×10^{-10}	Adding CNTs reduced pore size and oxide layer fraction in the electrolyte	[30]
7075 Al alloy	ZrO_2	2	Current density: 100mA/cm^2 Alkaline-silicate-molybdate electrolyte Coating time: 5min	6.95×10^{-10}	MoO_2 particles were added through Na_2MoO_4 salt decomposition, while ZrO_2 particles were included via electrophoresis and physical mixing with molten Al_2O_3 oxides.	[31]
Al-Zn-Mg	NH_4VO_3	3	Current density: 100mA/cm^2 Alkaline-aluminate-ZrO_2 electrolyte Coating time: 3min	295×10^{-11}	Introducing V_2O_5 via NH_4VO_3 ionization and ZrO_2 through electrophoresis and physical mixing has helped reduce structural flaws in the oxide layer.	This work

Table 4. Results of EIS Tests of the Oxide Layers Immersed in a 3.5 wt.% NaCl Solution for 1h

Sample	R_s (Ωcm^2)	R_o (Ωcm^2)	*CPE-*n_o	*CPE-*Y_o (S.s^n.cm^{-2})	R_i (Ωcm^2)	*CPE-*n_i	*CPE-*Y_i (S.s^n.cm^{-2})	W (S*S$^{1/2}$)
Bath A	17.54	6.21×10^5	0.79	5.77×10^{-8}	5.23×10^6	0.48	1.02×10^{-6}	7.83×10^{-6}
Bath B	17.62	8.24×10^6	0.81	4.01×10^{-9}	4.11×10^7	0.45	3.01×10^{-7}	2.00×10^{-6}

mitigating structural flaws within the oxide layer. Potentiodynamic polarization tests have underscored the superior corrosion resistance of the coating from Bath B, indicating a substantial shift to a more positive E_{corr} and a remarkably lower i_{corr} compared to Bath A. This difference highlights the enhanced corrosion protection afforded by the altered surface structure resulting from the incorporation of V_2O_5. The comprehensive study has demonstrated that the dual incorporation of ZrO_2 and V_2O_5 particles into the alumina layer not only influences the composition and morphology of the oxide layer but also significantly enhances the corrosion resistance of

the coated Al-Zn-Mg alloy. These findings hold promise for advancing the development of protective coatings for aluminum alloys, showcasing the potential of particle incorporation to tailor surface properties and improve overall performance.

Acknowledgements

This work was supported by the National Research Foundation of Korea (NRF) funded by the Korean Government (MSIT) (No. 2022R1A2C1006743).

Conflicts of Interest

The authors declare that they have no conflict of interest.

Author Contribution

Kaseem M contributed to conceptualization, data curation, formal analysis, funding acquisition, investigation, methodology, project administration, resources, validation, visualization, writing – original draft, writing – review & editing. Fattah-alhosseini A contributed to formal analysis, writing – original draft, writing – review & editing.

Abbreviation List

AFM, Atomic force microscopy
EDS, Energy-dispersive spectrometer
EIS, Electrochemical impedance spectroscopy
OCP, Open circuit potential
PEO, Plasma electrolytic oxidation
XPS, X-ray photoelectron spectroscopy
XRD, X-ray diffraction

References

[1] Allachi H, Chaouket F, Draoui K. Corrosion inhibition of AA6060 aluminum alloy by lanthanide salts in chloride solution. *J Alloys Compd*, 2009; 475: 300-303.[DOI]

[2] Zhu Z, Tu W, Cheng Y et al. The formation of metallic W and amorphous phase in the plasma electrolytic oxidation coatings on an Al alloy from tungstate-containing electrolyte, *Surf Coating Technol*, 2019; 361: 176-187.[DOI]

[3] Sankara Narayanan TSN, Park IS, Lee MH. Strategies to improve the corrosion resistance of microarc oxidation (MAO) coated magnesium alloys for degradable implants: prospects and challenges. *Prog Mater Sci*, 2014; 60: 1-71.[DOI]

[4] Kaseem M, Ko YG. Electrochemical Response of Al_2O_3-MoO_2-TiO_2 Oxide Films Formed on 6061 Al alloy by plasma electrolytic oxidation. *J Electrochem Soc*, 2016; 163: C587.[DOI]

[5] Zehra T, Kaseem M, Hossain S et al. Fabrication of a protective hybrid coating composed of TiO_2, MoO_2, and SiO_2 by plasma electrolytic oxidation of titanium. *Metals*, 2021; 11: 1182.[DOI]

[6] Nisar SS, Choe HC. Plasma electrolytic oxidation coatings on mechanically cold-worked titanium in solution containing hydroxyapatite ions. *Surf Coat Technol*, 2024; 479: 130524.[DOI]

[7] Wang P, Wu T, Peng H et al. Effect of $NaAlO_2$ concentrations on the properties of micro-arc oxidation coatings on pure titanium. *Mater Lett*, 2016; 170: 171-174.[DOI]

[8] Rehman Zur, Uzair M, Lim HT et al. Structural and electrochemical properties of the catalytic CeO_2 nanoparticles-based PEO ceramic coatings on AZ91 Mg alloy. *J Alloys Compd*, 2017; 726: 284-294.[DOI]

[9] Kaseem M, Kamil MP, Ko YG. Electrochemical response of MoO_2-Al_2O_3 oxide films via plasma electrolytic oxidation. *Surf Coat Technol*, 2017; 322: 163-173.[DOI]

[10] Movahedi N, Ali Habibolahzadeh A. Effect of plasma electrolytic oxidation treatment on corrosion behavior of closed-cell Al-A356 alloy foam. *Mater Lett*, 2016; 164: 558-561.[DOI]

[11] Gnedenkov SV, Khrisanfova OA, Zavidnaya AG et al. PEO coatings obtained on an Mg-Mn type alloy under unipolar and bipolar modes in silicate-containing electrolytes. *Surf Coat Technol*, 2010; 204: 2316-2322.[DOI]

[12] Srinivasan PB, Liang J, Balajeee RG et al. Effect of pulse frequency on the microstructure, phase composition and corrosion performance of a phosphate-based plasma electrolytic oxidation coated AM50 magnesium alloy. *Appl Surf Sci*, 2010; 256: 3928-3935.[DOI]

[13] Arunnellaiappan T, Ashfaq M, Krishna LR et al. Fabrication of corrosion-resistant Al_2O_3-CeO_2 composite coating on AA7075 via plasma electrolytic oxidation coupled with electrophoretic deposition. *Ceram Int*, 2016; 42: 5897-5905.[DOI]

[14] Bahramian A, Raeissi K, Hakimizad A. An investigation of the characteristics of Al_2O_3/TiO_2 PEO nanocomposite coating. *Appl Surf Sci*, 2015; 351: 13-26.[DOI]

[15] Xiang N, Song RG, Zhuang JJ et al. Effects of current density on microstructure and properties of plasma electrolytic oxidation ceramic coatings formed on 6063 aluminum alloy. *Trans Nonferrous Met Soc China*, 2016; 26: 806-813.[DOI]

[16] Fatimah S, Kamil MP, Kwon JH et al. Dual incorporation of SiO_2 and ZrO_2 nanoparticles into the oxide layer on 6061 Al alloy via plasma electrolytic oxidation: Coating structure and corrosion properties. *J Alloys Compd*, 2017; 707: 358-364.[DOI]

[17] Kwon JH, Fatimah S, Baek SH et al. Electrochemical response of VxOy-Al_2O_3 composite layer with dark-green color achieved by plasma electrolytic oxidation. *J Alloys Compd*, 2020; 827: 154367.[DOI]

[18] Fatimah S, Yoon DK, KoYG. Role of V_2O_5 particles on the microstructures and corrosion behavior of Al-Mg-Si alloy via plasma electrolysis. *J Mater Res Technol*, 2020; 284: 116757.[DOI]

[19] Kaseem M, Ko YG. On the compactness of the oxide layer induced by utilizing a porosification agent. *Appl Surf Sci*, 2019; 473: 715-725.[DOI]

[20] Fattah-alhosseini A, Chaharmahali R, Babaei K. Effect of particles addition to solution of plasma electrolytic oxidation (PEO) on the properties of PEO coatings formed on magnesium and its alloys: A review. *J Magnes Alloys*, 2020; 8: 799-818.[DOI]

[21] Shin KR, Ko YG, Shin DH. Influence of zirconia on biomimetic apatite formation in pure titanium coated via plasma electrolytic oxidation. *Mater Lett*, 2010; 64: 2714-2717.[DOI]

[22] Narayanan T, Lee M. Incorporation of ZrO_2 particles in the oxide layer formed on Mg by anodizing: influence of electrolyte concentration and current modes, *J Alloys Compd* 853, 2021; 157036.[DOI]

[23] Marques IDSV, Da Cruz NC, Landers R et al. Incorporation of Ca, P, and Si on bioactive coatings produced by plasma electrolytic oxidation: The role of electrolyte concentration and treatment duration. *Biointerphases*, 2015; 10: 041002.[DOI]

[24] Kaseem M, Zehra T, Khan MA et al. Guar gum-driven high-energy plasma electrolytic oxidation for concurrent improvements in the electrochemical and catalytic properties of Ti-15 Zr alloy. Surf Interfaces, 2022; 34: 102403.[DOI]

[25] Kaseem M, Hussain T, Rehman ZU et al. Advantage of an in-situ reactive incorporation over direct particles incorporation of V_2O_5 for a competitive plasma electrolysis coating. *Surf Coat Technol*, 2020;

399: 126200.[DOI]

[26] Safira AR, Kaseem M. Interfacial and electronic modulation of M-bridged heterostructures with L-tryptophan and transition metallic oxides: Enhancing corrosion resistance and photocatalytic activity. *ACS Appl Mater Interfaces*, 2023; 15: 5906-59825.[DOI]

[27] Bayati M, Zargar H, Molaei R et al. MAO-synthesized Al_2O_3-supported V_2O_5 nano-porous catalysts: growth, characterization, and photoactivity. *Appl Surf Sci*, 2010; 256: 3806-3811.[DOI]

[28] Kim GW, Kim YS, Yang HW et al. Influence of ZrO_2 incorporation into coating layer on electrochemical response of low-carbon steel processed by electrochemical plasma coating. *Surf Coat Technol*, 2015; 269: 314-318.[DOI]

[29] Stern M, Geary AL. A theoretical analysis of the shape of polarization curves. *J Electrochem Soc*, 1957; 104: 56-63.[DOI]

[30] Lee KM, Jo JO, Lee ES et al. Incorporation of carbon nanotubes into oxide layer on Al-Zn-Mg alloy by plasma electrolytic oxidation. *J Electrochem Soc*, 2011; 158: C325-C328.[DOI]

[31] Kaseem M, Lee YH, Ko YG. Incorporation of MoO_2 and ZrO_2 particles into the oxide film formed on 7075Al alloy via micro-arc oxidation. *Mater Lett*, 2016; 182: 260-263.[DOI]

[32] Zehra T, Pital SA, Shrestha NK et al. Anionic assisted incorporation of WO3 nanoparticles for enhanced electrochemical properties of AZ31 Mg alloy coated via plasma electrolytic oxidation. *J Alloys Compd*, 2022; 916: 165445.[DOI]

[33] Rehman ZUr, Shin SH, Lim HT et al. Transformation of plasma electrolytic oxidation coatings from crater to clyuster-based structure with increase in DC voltage and the role of ZrO_2 nanoparticles. *Surf Coat Technol*, 2017; 311: 383-390.[DOI]

[34] Kaseem M, Safira AR, Aadil M et al. Innovative approach to boosting the chemical stability of AZ31 magnesium alloy using polymer-modified hybrid metal oxides. *J Alloys Compd*, 2024.[DOI]

[35] Molaei M, Fattah-alhosseini A, Nouri M et al. Enhancing cytocompatibility, antibacterial activity and corrosion resistance of PEO coatings on titanium using incorporated ZrO_2 nanoparticles. *Surf Interfaces*, 2022; 30: 1019687.[DOI]

[36] He D, Li G, Shen D, Guo C et al. Effect mechanism of ultrasound on growth of micro-arc oxidation coatings on A96061 aluminum alloy. *Vacuum*, 2014; 107: 99-102.[DOI]

Brief of Corresponding Author(s)

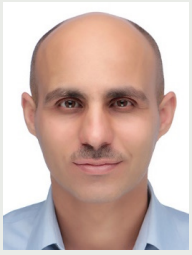

Mosab Kaseem

He is an Assistant Professor at the Department of Nanotechnology and Advanced Materials Engineering, Sejong University, Republic of Korea since 2018. He earned his Ph.D. From 2013 to 2017, and served as a Research Professor at the School of Materials Science and Engineering, Yeungnam University, Republic of Korea. Dr. Kaseem's research focuses on advancing surface characteristics of light metals through plasma electrolysis, tailoring metallic biomaterial surfaces, and exploring the synthesis, properties, and applications of biodegradable polymer blends. He has produced over 120 publications in esteemed journals, with an h-index of 38.

Arash Fattah-alhosseini

He is a Professor of Materials Engineering at Bu-Ali Sina University in Iran. He earned M.Sc. and Ph.D. at Isfahan University of Technology (IUT). His research focuses on the development of novel coatings via Plasma Electrolytic Oxidation (PEO) and Physical Vapor Deposition (PVD), which are useful in the fields of corrosion and surface engineering. Over the past few years, he has established a vigorous research program in the area of photocatalysis, focusing on PEO coatings, characterization, and environmental and energy-related applications. He has published more than 235 ISI papers, earning an h-index of 44.